Tidal range resource of the Patagonian shelf

Vicky Martí Barclay [a],*, Simon P. Neill [a], Athanasios Angeloudis [b]

[a] *School of Ocean Sciences, Bangor University, Menai Bridge LL59 5AB, UK*
[b] *School of Engineering, Institute for Infrastructure & Environment, University of Edinburgh, Edinburgh EH9 3FG, UK*

ARTICLE INFO

ABSTRACT

With vast potential for renewable energy conversion, the ocean could help reduce our reliance on fossil fuels. Of the various forms of ocean energy, tidal range power is both mature and predictable, dating back to 1966. However, only a few regions of the world are suited to tidal range power. Here, we examine the tidal range potential of the Patagonian shelf – estimated to contain over 100 GW of tidal dissipation. We use a high resolution global tidal atlas (TPXO9) to examine this resource from theoretical and technical perspectives. The theoretical resource is 913 TWh (104 GW) – considerably exceeding neighbouring Argentina's electricity demand ($\sim$ 143 TWh in 2021). We find that due to near-resonance with the semidiurnal tides, the resource is concentrated in two regions – Golfo de San Matías, and Bahía Grande to Río Grande. Three sites are chosen for further analysis after considering practical constraints such as water depth and proximity to the electricity grid. Through 0D modelling with tidal range power plant operation we find that the selected sites offer high energy extraction potential, exceeding 40% of the available resource. Further analysis shows how the combination of the sites can reduce the periods of no-generation to under 20%.

1. Introduction

The majority of electricity produced on Earth derives from the Sun.[1] This includes the combustion of fossil fuels (61.5% of global electricity production in 2020 [1]) formed from the remains of organic matter produced by photosynthesis, and hydro (16.6% in 2020), based on rainfall, driven by weather governed by a global redistribution of the Sun's energy. However, one exception, and a resource that has significant global potential, is tidal power, which relies on the gravitational pull of the Moon, in combination with the Earth's rotation.[2] There are two main ways that the energy of the tides can be converted into electricity – either by intercepting regions of strong tidal flow via in-stream tidal generators [2], or by exploiting the potential energy of the tides through tidal range power plants [3]. It is the tidal range resource, and the development of associated tidal range power plants, that are the focus of this study.

Converting tidal range energy into other useful forms of energy is not a new concept – there is evidence of tide mills extending back to medieval times [4]. However, only since 1966 has tidal energy been used to produce electricity [3]. A tidal range power plant is based on the construction of an artificial embankment that impounds a large volume of water. In all existing tidal range power plants, such as La

Rance in Brittany [5], this embankment spans the entire width of an estuary or channel, known as a *tidal barrage*. However, barrages proposed to date have high capital costs due to their scale and are associated with significant environmental impacts, including near- and far-field effects [6]. A concept that has been proposed more recently is that of a *tidal lagoon* – an embankment that generally only partially impounds a smaller section of an estuary or bay. Typically, tidal lagoons impound a smaller volume of water than a barrage, and therefore correspond to lower capital cost and lower environmental footprint. Although no lagoon has yet been built, the concept considerably extends the opportunities for tidal range, since an estuary or channel is no longer required for the construction of the power plant [2].

If we consider first the simplest mode of tidal range power plant operation, i.e. ebb-generation – during the flood phase of the tidal cycle, water enters the impoundment through sluice gates and idling turbines. At high water, sluice gates and turbine wicket gates are closed and the water is held inside the impoundment – a time period known as 'holding'. The water level outside the impoundment naturally ebbs, and once sufficient head is generated water is directed through the turbines to turn a generator and produce electricity. Other modes of operation include flood-generation and two-way operation – the latter of which can be used to reduce variability, especially when combined with pumping [7].

---

[1] The only real exceptions are geothermal and nuclear power plants.
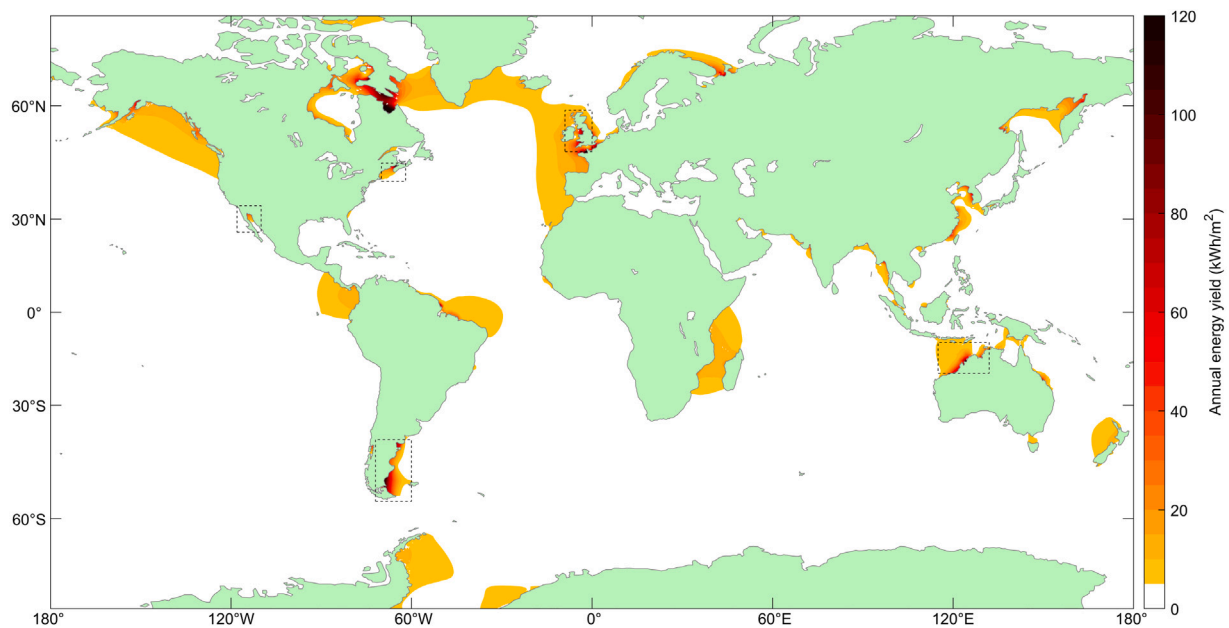[2] Although the Sun also has an important contribution to the tides.

Fig. 1. Global annual energy yield (kWh/m²) with no bathymetric constraints based on the analysis of TPXO9-v4 (refer to Section 3 for the methods). The same constraints as in Neill et al. (2021), i.e. <30 m depth, minimum 50 kWh/m², and exclusion of the Hudson Bay due to challenges with extensive ice cover, are applied. Boxed regions highlight areas of high tidal range energy that have previously been studied.

Global tidal dissipation has been estimated as 2.4 TW, the majority of which (1.6 TW) occurs in the shelf seas [8]. In many of these shelf regions, tidal resonance leads to localised amplification of the tides [2], and hence considerably elevated tidal ranges, such as the 16 m spring tidal range experienced in the Bay of Fundy, Canada – the highest tidal range in the world [9]. The global tidal range resource has been estimated as 9115 TWh [10] – enough to provide over 36% of global demand for electricity.[3] For comparison with this figure, calculated using TPXO9-v2, we recalculate (refer forwards for methods) the global theoretical resource (Fig. 1) but using a more recent version of TPXO9, v4. The recalculated global tidal range resource is 9220 TWh, an increase of only 105 TWh compared to the previous figure by Neill et al. (2021). This 1% variation is not significant and no obvious changes in the distribution of the resource are observed. The resource is concentrated in a few regions, including the Bay of Fundy in Canada, the NW European shelf, the NW Australian shelf, and the Patagonian shelf. Previous studies have examined the first three of these regions in detail from both theoretical and technical tidal range perspectives, but no study has yet examined the potential of tidal range power plants in the Patagonian shelf other than in one specific location [11].

Tidal range energy has been previously considered in Argentina. The first idea was proposed as early as 1915 and at least six other projects were put forward for consideration before the 1990s, at which point interest waned [11,12]. These projects mostly focused on one area, Peninsula Valdés. This peninsula is in the southeast extremity of Golfo de San Matías and forms two smaller gulfs at either side of it, creating an interesting location for tidal barrages. The projects ranged in size, from 600 to 5300 MW, and in design, from closing one gulf with a barrage; closing both gulfs; and even creating a canal across the isthmus, thus connecting both gulfs and making the most of the tidal phase difference on either side of the isthmus [12]. Additionally, one of these studies identified other areas of interest for exploiting tidal energy, such as Ría de Gallegos (1900 GWh/year), Ría de Santa Cruz (3700 GWh/year) and other less energetic locations [12]. The prohibitive construction costs and the predicted environmental impacts meant none of the projects were continued.

Table 1
Argentina's 2021 electricity matrix. Renewable includes biomass, biogas, wind, solar and small-scale hydropower, noting that large scale hydro has its own category. Data from CAMMESA (Argentine Wholesale Electricity Market Clearing Company) [13].

Source	GWh	%
Fossil fuels	90,074	63.2
Hydropower	24,116	16.9
Renewable	17,437	12.2
Nuclear	10,170	7.1
Import	819	0.6
Total	**142,616**	**100**

The Patagonian shelf extends 1500 km along the coastline of Argentina. Argentina relies heavily on fossil fuels for its electricity generation, including many "off-grid" communities that rely on expensive diesel (3% of fossil fuel generation). In 2021, 12.2% of Argentina's electricity generation was from renewable sources (excluding large-scale hydro) and 17% from large-scale hydropower, but 63.3% was from the combustion of fossil fuels and the remaining 7.1% was nuclear power (Table 1) [13]. However, with a potentially significant tidal range potential as identified in Neill et al. [3], this study investigates the contribution that tidal range could have on the energy mix for the region.

Although past studies have examined some aspects of the physical oceanography of the Patagonian shelf (e.g. [14–19]), no study has specifically examined the theoretical or technical tidal range resource of the region. Further, no study has examined the practical constraints to tidal energy development of the region, nor optimised tidal range power plant operation to investigate if it is a feasible form of energy conversion for the region. Here, we use a global tidal atlas (TPXO9-v4) to investigate the theoretical tidal range resource of the Patagonian shelf. By selecting locations feasible for tidal energy conversion (from both theoretical and practical perspectives), we investigate the technical resource extraction prospects in the most promising regions in more detail.

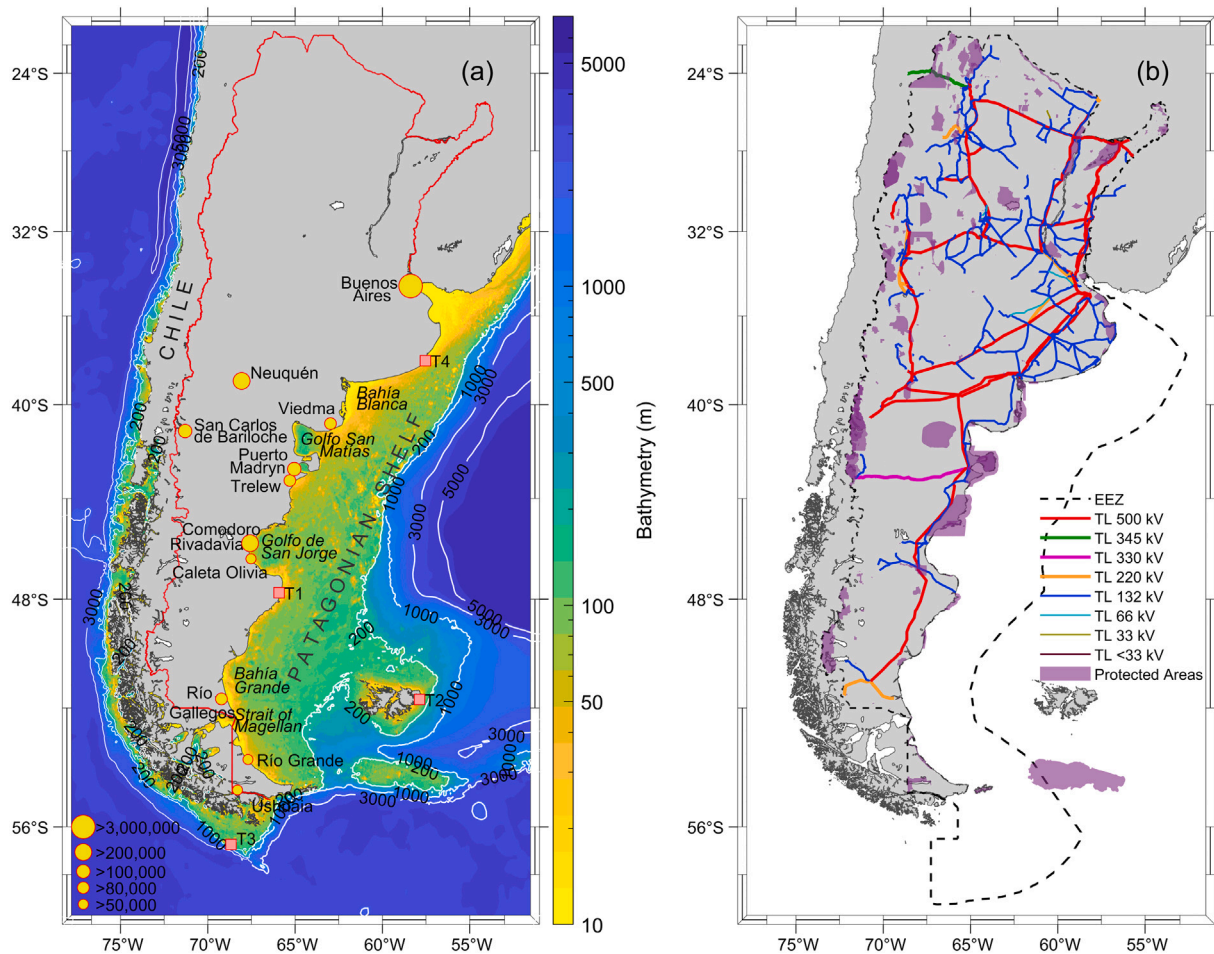[3] Global electricity consumption in 2020 was 24,901.4 TWh [1].

Fig. 2. (a) Bathymetry (metres) around Argentina and Chile on a log scale and contour lines showing the continental shelf boundary (200 m) and continental slope (1000–5000 m). Bathymetry data from TPXO9-v4, sourced from Smith and Sandwell v18.5, SRTM15+ (Shuttle Radar Topography Mission) and IBSCO v1.0 (International Bathymetric Chart of the Southern Ocean). T1–T4 are the tide gauge stations used for local validation of TPXO9. Yellow circles are scaled to population size (see legend southwest corner). (b) EEZ (Exclusive Economic Zone) boundary for Argentina as dashed black line; Transmission lines are the solid lines; and the protected areas are purple patches. Transmission lines and protected areas data from Instituto Geográfico Nacional de la República Argentina [20]. Note that the Falkland Islands/Islas Malvinas have been excluded from the EEZ as it is considered a disputed territory.

2. Study region – Patagonia

Patagonian shelf tides

The Patagonian Continental Shelf ($38°S - 55°S$) is the southernmost part of the SW Atlantic shelf. It varies in width, being narrowest in the northern sector (ca. 200 km) and between 400 and 600 km at most points (Fig. 2a). Water depth varies considerably along the coastline. The northern section (Buenos Aires to Bahía Blanca) is mostly shallow, with depths below 50 m. South of Bahía Blanca the coastline is more abrupt and generally deeper. For example, water depths in the Golfo San Matías and Golfo de San Jorge generally exceed 100 m. There is a generally gentle and smooth gradient from the coastline until the edge of the shelf at the 200 m isobath. These characteristics suggest the Patagonian shelf could be a system that is in near-resonance [21–24]. This is reflected in the large tidal amplitudes observed along the Patagonian coastline (Fig. 3), that reach ca. 4 m for the M2 (principal lunar semidiurnal) tide and ca. 1 m for both the S2 (principal solar semidiurnal constituent) and the N2 (larger lunar elliptic semidiurnal) at around 51°S, in Bahía Grande. The highest M2 amplitudes (3.86 m) are found in the Río Gallegos estuary, whilst the largest S2 and N2 amplitudes are observed in the north of Bahía Grande and in the Strait of Magellan, where they reach 1.00 m. Regarding the main diurnal

constituents (K1 and O1, Fig. 4), they also reach their highest values, 0.25 m and 0.23 m respectively, in Bahía Grande.

There are three main semidiurnal amphidromic points (Fig. 3), which agrees with previous studies [15,16,18,19]. The semidiurnal tidal wave enters the area from the south-southeast and rotates clockwise around the amphidromes, with the phases propagating northwards along the coast. The diurnal tides only rotate around one amphidrome, located in the northern half of the Patagonian shelf (Fig. 4).

As progressive waves travel into shelf sea regions they are often reflected at the coast, particularly in bays and estuaries. The interaction between the incoming wave and the reflected wave creates a standing wave. A standing wave is a combination of two progressive waves with the same amplitude travelling in opposite directions. In a standing wave system the amplitudes and currents are 90° out of phase, i.e peak currents occur mid-tide and slack water coincides with high and low water [25]. Due to these characteristics, there is no net energy flux in a perfect standing wave system. Along the Patagonian shelf the M2 tidal system is a combination of progressive and standing waves (Fig. 5a). The regions where standing waves dominate roughly coincide with those found by Glorioso and Flather [16], particularly in Golfo San Matías and Bahía Grande. This suggests tidal wave reflections constructively interfere at the three main bays, leading to a near-resonant state in Golfo San Matías and Bahía Grande, where the highest M2 amplitudes are found.
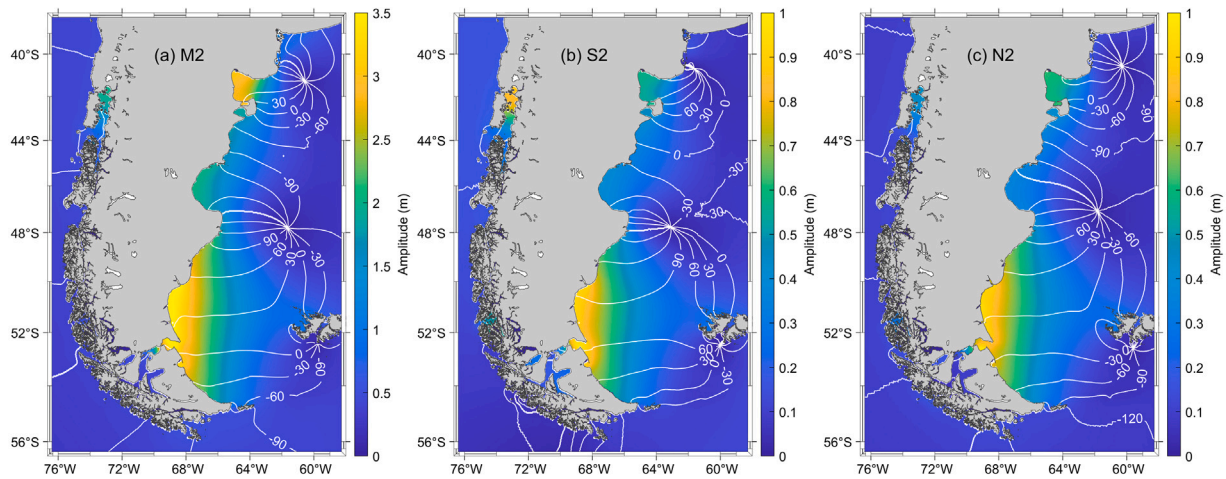
Fig. 3. Co-tidal charts for the three dominant semi-diurnal tidal constituents along the Patagonian shelf (a) M2, (b) S2, (c) N2. Colour scale is amplitude in metres; and white contours are co-tidal lines, connecting regions that are equal in tidal phase plotted every 30°. Data from TPXO9-atlas-v4.
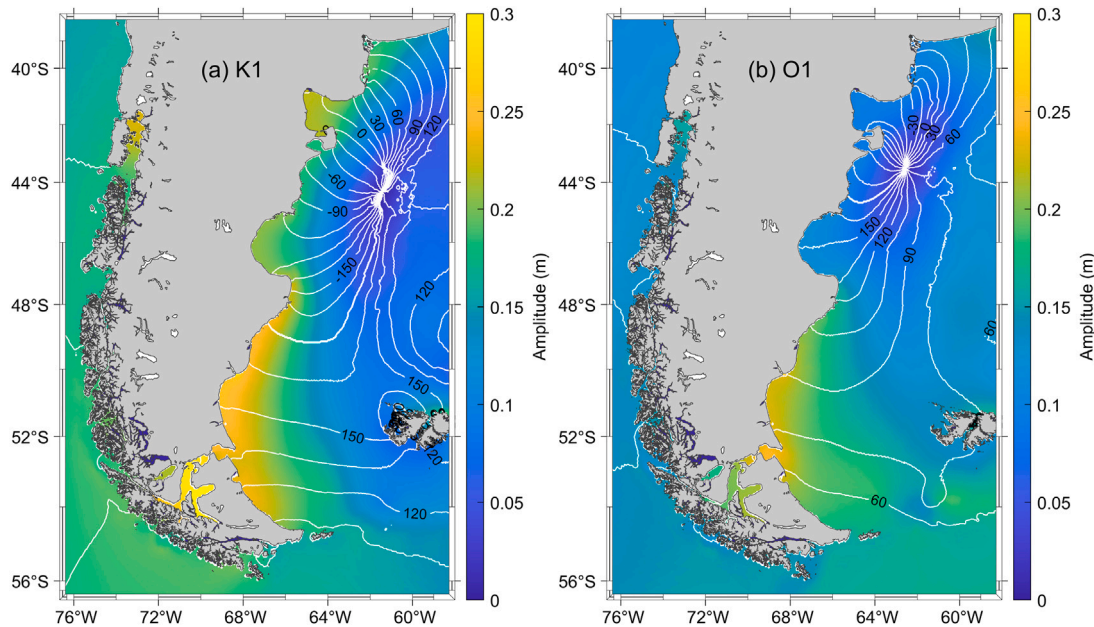

Fig. 4. Co-tidal charts for the two dominant diurnal tidal constituents along the Patagonian shelf (a) K1 and (b) O1. Colour scale is amplitude in metres. White contours are co-tidal lines, connecting regions that are equal in tidal phase plotted every 15°. Data from TPXO9-atlas-v4.

The dominance of the semidiurnal tides along the Patagonian shelf is also confirmed by the Form Factor[4] (*F*, Fig. 5b), which is below 0.25 along the shore, and away from amphidromic points. There is a slight difference between Golfo San Matías, Golfo de San Jorge, and Bahía Grande. The lowest value for *F* is found in Golfo San Matías, suggesting diurnal tides will play less of a role in this area. Additionally, a spring-neap ratio is calculated to assess the lunar variability of the tidal cycle (Fig. 5c). This ratio is computed as in Robins et al. [26]:

$$R = 1 - \frac{H_{S2}}{H_{M2}} \tag{1}$$

where H_{S2} and H_{M2} are the amplitudes of the S2 and M2 tides at each grid cell. A high value of *R* indicates the M2 tide dominates over the S2. When this happens, it is likely that the spring and neap tides are similar. In contrast, lower ratios mean there will be a larger difference between spring and neap tidal ranges. The spring-neap ratio varies along the

Patagonian coastline; in Golfo San Matías it is ca. 0.80 whilst in Bahía Grande it is ca. 0.75. Both the form factor and spring-neap ratio are important regarding energy output. They can hint as to how consistent power output will be at diurnal and weekly timescales.

Argentinian grid system

The Argentinian transmission network, called Sistema Argentino de Interconexión (SADI) in Spanish (Fig. 2b), is subdivided into two components: a high-voltage transmission network between electric regions operating at 500 kV, and a lower voltage network (33 kV to 400 kV) that connects generators, distributors and large consumers within regions. The former is 14,197 km in length (with an additional 723 km of inter-region connection at 132–220 kV), whilst the latter is 21,472 km [13]. The transmission network extends from the north of the country down to the Patagonia region; however, it does not reach the archipelago of Tierra del Fuego, the southernmost region of Argentina, which is separated from the mainland by the Strait of

---

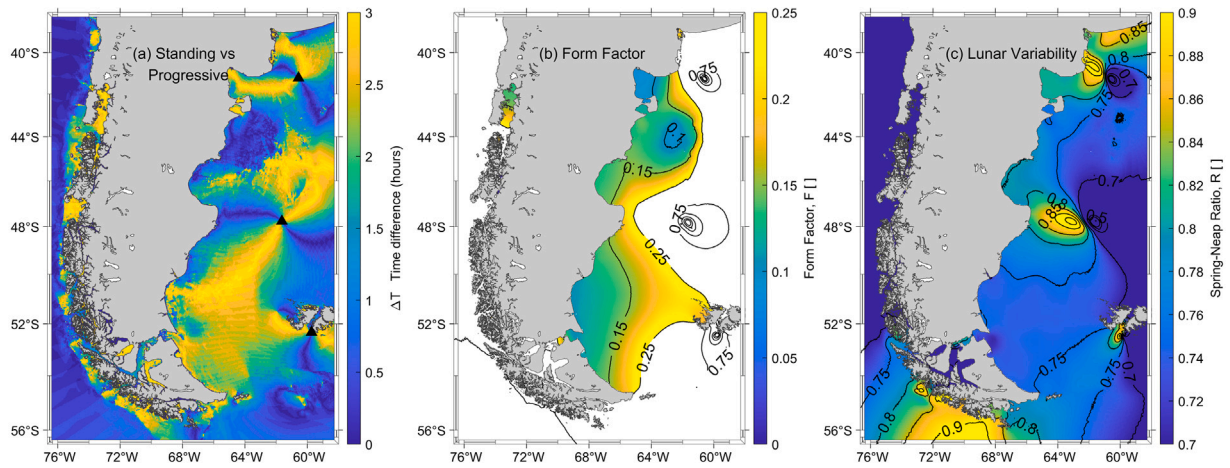[4] The ratio between diurnal and semidurnal tidal amplitudes.

Fig. 5. (a) Time difference (ΔT) in hours between the second M2 high water and closest peak M2 current speeds on the Patagonian shelf. In a standing wave system ΔT is maximum and in a progressive wave system ΔT < 1 h. Black triangles indicate M2 amphidromic points. (b) Form Factor (*F*) for the Patagonian shelf, showing the ratio between diurnal and semi-diurnal tides ($F = (H_{K1} + H_{O1})/(H_{M2} + H_{S2})$). Tides are semidiurnal ($F < 0.25$); mixed, mainly semidiurnal ($0.25 < F < 1.5$); mixed, mainly diurnal ($1.5 < F < 3.0$); or diurnal ($F > 3.0$). Colour scheme is masked to 0.25 to capture the smaller differences and complete range of F is visible through the black contours. (c) Spring-Neap ratio (*R*) for the Patagonian shelf computed as $R = 1 - (H_{S2}/H_{M2})$. Black contours (also spring-neap ratio) are to aid visualisation.

Magellan. This is relevant since it is not necessary to consume the electricity in the same area as it is generated.

Despite Buenos Aires, the capital city of Argentina, being one of the most populated cities in the world, Argentina has a very low population density. Nearly 50% of the population is concentrated in ten big urban agglomerations in the north of the country. In contrast, the Patagonia region is very sparsely populated, with ca. 2.5 m people living in over 800,000 km^2. There are several cities with a population over 90,000 and a few between 30,000 and 90,000. These are all connected to the SADI, except for Ushuaia and Río Grande, both in Tierra del Fuego. These two cities do not have a grid connection between one another, but they each have a small distribution network that transports electricity to neighbouring areas.

3. Methods

3.1. Global tidal atlas, TPXO

TPXO9-atlas-v4 is a global tidal atlas with a $1/30° \times 1/30°$ resolution obtained from the combination of a $1/6° \times 1/6°$ global tidal solution and local solutions of $1/30° \times 1/30°$ resolution for all coastal areas [27]. For the global resource estimation, five constituents are used (M2, S2, N2, K1 and O1). The regional calculations were carried out initially using 5 tidal constituents (M2, S2, N2, K1 and O1), and later 14 constituents (Table 2) (M2, S2, N2, K1, O1, K2, 2N2, MF, MM, Q1, P1, MS4, MN4, M4) to explore the importance of other constituents on the annual potential energy magnitude and the tide variability (e.g. quarter diurnal constituents).

The TPXO9-v4 dataset was compared to tidal constituents obtained from tidal analysis of water level time series at four tide gauges (Fig. 2a) distributed throughout the study region. This validation (Table 3) demonstrated excellent agreement between the *in situ* data from GESLA (Global Extreme Sea Level Analysis [28,29]) and TPXO9-v4 for both amplitudes and phases for the four main tidal constituents, with RMSE (root-mean-square-error) in the range $2-3$ cm (amplitude) and $3-12°$ (phase).

3.2. Theoretical resource assessment

The theoretical tidal range resource is calculated following the method outlined in Neill et al. [10]. The amplitudes and phases for the different tidal constituents from the TPXO9 solution are used to

obtain the elevation time series at each grid cell for an arbitrary year (2020) using *T_TIDE* [30]. Elevations are predicted using different time steps to test the sensitivity to this parameter. The predictions are calculated using 5, 15, 30 and 60 min increments for both the 5 and 14 tidal constituent calculation. The aggregated annual potential energy is calculated at each grid cell over both flood and ebb phases of the tidal cycle as:

$$E_{\max} = \sum_{i=1}^{n} \frac{1}{2} \rho g A R_i^2 \tag{2}$$

where the subscript *i* denotes each successive rising or falling tide, ρ is the density of seawater (1025 kg/m^3), g is acceleration due to gravity, R is the tidal range of each half tidal cycle, and A the area of the grid cell. For $n \approx 1411$, i.e. the number of tidal range R transitions over a year, the annual energy density $PE = E_{\max}/A$ is in turn calculated in units of kWh/m^2.

The values presented in Section 4.1.1 are the total annual theoretical potential energy of an area. However, these are constrained to water depths of less than 30 m and an energy density of at least 50 kWh/m^2 to present a more realistic estimation and for consistency with the methodology applied by Neill et al. [10]. Deeper waters and lower energy yields would not be commercially viable [3].

While tides vary in time, a year is a sufficient period for representative tide conditions, as discussed in Pappas et al. [31]. The difference between using 5 or 14 constituents at the regional scale (Patagonian shelf) is negligible to the magnitude of the resource, no greater than 5 kWh/m^2 at a single cell and <1% difference of the total resource. Regarding the time steps used, the maximum difference in magnitude is <4 kWh/m^2 when comparing results at 60 min with the finest resolution (5 min) and <1 kWh/m^2 for 15 and 30 min (compared to 5), equivalent to <3% and <1% of the total resource respectively. The results in the following sections are obtained using the highest resolution, i.e. 14 constituents and 5 min time stamp. Including these constituents captures the tide variability that a plant operation may need to account in quantifying the technically extractable resource.

3.3. Technically extractable resource assessment

The extractable resource assessment makes use of the 0D modelling methodology of Angeloudis et al. [32]. The methodology is underpinned by:

Table 2

Description of the 14 tidal constituents used for the analysis of the resource on the Patagonian shelf. Period of the constituents expressed in hours. Spatial mean amplitude over the Patagonia shelf in metres is restricted to the 200 m shelf break and between 40°S and 56°S.

Constituent	Description	Period (h)	Mean amplitude (m)
M2	Principal lunar semidiurnal constituent	12.42	1.086
S2	Principal solar semidiurnal constituent	12.00	0.262
N2	Larger lunar elliptic semidiurnal constituent	12.66	0.268
K1	Lunar diurnal constituent	23.92	0.129
O1	Lunar diurnal constituent	25.84	0.124
K2	Lunisolar semidiurnal constituent	11.96	0.072
2N2	Lunar elliptical semidiurnal second-order constituent	12.90	0.039
Q1	Larger lunar elliptic diurnal constituent	26.88	0.029
P1	Solar diurnal constituent	24.04	0.036
MF	Lunisolar fortnightly constituent	322.58	0.015
MM	Lunar monthly constituent	666.67	0.008
M4	Shallow water overtides of principal lunar constituent	6.21	0.044
MN4	Shallow water quarter diurnal constituent	6.27	0.018
MS4	Shallow water quarter diurnal constituent	6.11	0.022

Table 3

Comparison of amplitude (α in m) and phase (ϕ in degrees relative to Greenwich) of the four major tidal constituents (M2, S2, K1, O1) between *in situ* (GESLA) time series and TPXO9 at four locations around the Patagonian shelf (locations shown on Fig. 2a). The right hand column shows the length of time series used for tidal analysis at each station.

| Station	Ref.	Lon.	Lat.		M2		S2		K1		O1		Length (days)
					α [m]	ϕ [°]	α [m]	ϕ [°]	α [m]	ϕ [°]	α [m]	ϕ [°]	
Puerto Deseado	T1	294.09	−47.75	GESLA	1.75	132	0.33	193	0.24	196	0.19	136	437
				TPXO	1.77	138	0.33	191	0.22	201	0.16	121	
Port Stanley	T2	302.07	−51.75	GESLA	0.44	275	0.16	304	0.14	107	0.17	050	972
				TPXO	0.40	272	0.15	304	0.11	105	0.13	061	
Diego Ramírez Islands	T3	291.33	−56.56	GESLA	0.40	230	0.04	253	0.19	092	0.17	065	196
				TPXO	0.41	230	0.03	242	0.18	098	0.15	052	
Mar del Plata	T4	302.47	−38.04	GESLA	0.35	303	0.06	016	0.16	161	0.18	086	742
				TPXO	0.36	304	0.05	006	0.11	154	0.16	075	
				RMSE	0.02	003	0.01	008	0.03	005	0.03	012	
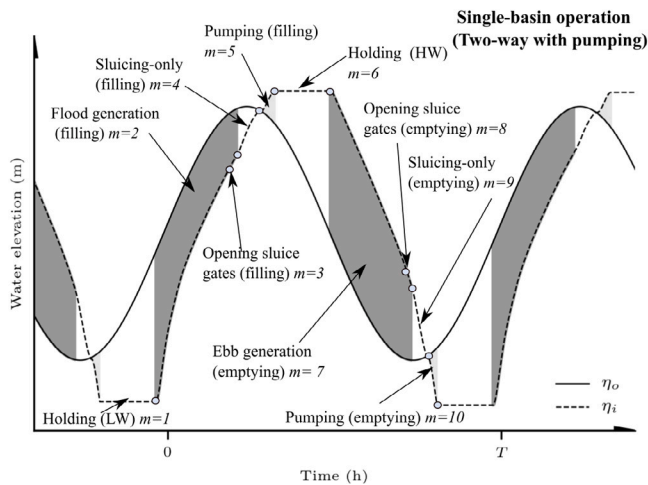
Fig. 6. Tidal power plant operation for a single basin scheme with two-way generation with pumping. Regions shaded in grey represent time periods when power is generated [10].

- principles of mass balance discretised in time through a finite difference approach. This describes the volume exchange between the sea and the impounded area, serving as a route to simulate water elevation changes relative to the sea [33].
- hydraulic structure parameterisations to represent sluice gate and turbine operation with respect to flow-rates and power generation. Sluice gates are represented using the orifice equation, while turbines through Hill chart approaches following Aggidis and Feather [34].

- condition-based operation rules to simulate the functioning of tidal power plants as they switch modes of operation with the evolving tidal conditions (Fig. 6)

The combination of these features leads to a 0D operation modelling approach, appropriate for preliminary assessments and sensitivity analyses of tidal power plant configurations [35]. Limitations of the 0D modelling emerge in neglecting any changes in the hydrodynamics by the presence of large-scale infrastructure, as considered in the studies of [36,37] or [38]. This can be addressed through 2D (or possibly 3D) shallow water equation hydrodynamic modelling once prospective projects are better defined [39]. The integration with the hydrodynamics enables the quantification of hydro-environmental [40] and ecological [41] impacts incurred by the introduction of the infrastructure within the marine environment. In addition, as 0D modelling is a form of simplified reservoir routing, it assumes a horizontal water surface within the impoundment. As such, there is an expected error that increases in designs that impound significant intertidal zones or encompass a large enough area for this assumption to neglect substantial 'wedge' storage volumes.

In the absence of detailed tidal power plant proposals, the analysis herein omits consideration of the hydrodynamics and assumes any installed capacities would be deployed at a small enough scale to not substantially alter the regional tidal hydrodynamics and challenge the sensible application range of 0D modelling. Nevertheless, for a consistent assessment of the performance of schemes of a given tidal power plant impounded area at sites of different energy density, we consider that the capacity C will vary as

$$C = \eta \frac{\rho g \bar{A}_s \bar{R}^2}{T C_F}, \qquad (3)$$

where η is the expected power plant efficiency, $\bar{A}_s$ the mean surface area, $\bar{R}$ the mean tidal range, which is assumed to converge to the average starting head difference $\bar{H}$, and C_F is the desirable capacity
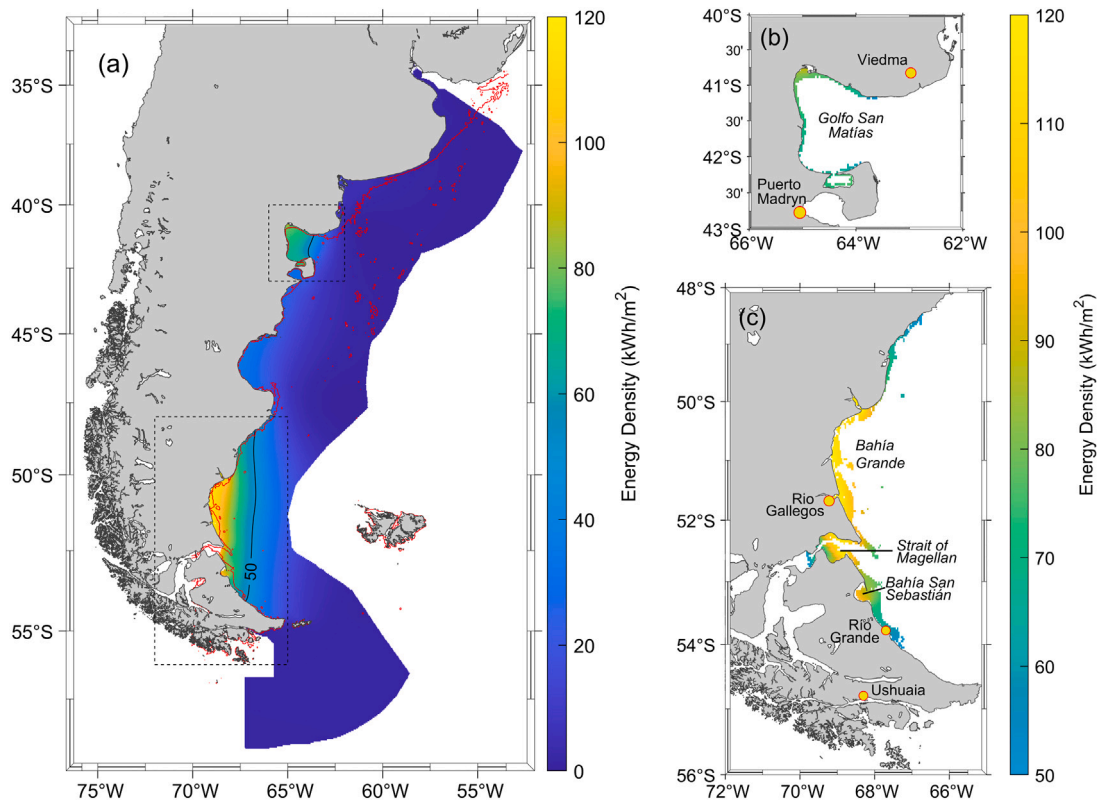
Fig. 7. Theoretical tidal range resource (kWh/m^2) along the Patagonian shelf: (a) for the entire Argentina EEZ (Exclusive Economic Zone). The 30 m isobath is represented with a red contour line and the 50 kWh/m^2 with a black contour line. Boxed regions are shown in right-hand side panel. (b, c) zoomed in areas where depth <30 m and annual energy density exceeds 50 kWh/m^2.

factor. The values of $\eta = 0.40$ and $C_F = 0.20$ are selected in this analysis. This simplified approach follows preceding technical resource assessment studies in the Gulf of California [42] and western Australia [3]. In particular, the capacity of the turbines for each site is tailored to the available resource by setting the turbine rated head to $0.8\bar{R}$. Finally, in relation to operation control, we consider two-way generation without and with the support of pumping intervals, as dictated over time following a 2-cycle energy maximisation optimisation applying the approach of [43]. This strategy acknowledges that the regulation of turbines and sluice gates will be adapted over time, as per the evolving tidal conditions in order to maximise performance.

4. Results

4.1. Patagonian tidal range resource

We first present the theoretical resource, which is defined as the maximum available potential energy [44]. In the following section we introduce the technical resource, which is the proportion of the theoretical resource that can be extracted using tidal range energy technology, and therefore takes into account device efficiencies and constraints [44]. Finally, we discuss aspects of the practical resource in Section 5, which considers external constraints that influence tidal energy conversion, such as water depth, minimum energy yield, the proximity to a grid connection, population or marine protected areas.

4.1.1. Theoretical resource

The theoretical tidal resource within the Argentinian EEZ is 12,405 TWh (Fig. 7). This reduces to 912.7 TWh once the bathymetric (<30 m) and minimum energy yield (50 kWh/m^2) constraints are applied. As expected from examining co-tidal charts, the theoretical resource is concentrated in two main areas along the Patagonian shelf:

Golfo San Matías (GSM) (41 − 42°S) and Bahía Grande to Río Grande (50 − 54°S).

The GSM bay has an average energy density of 64.9 kW/m^2 and contributes 1126.7 TWh (9%) of the total theoretical resource. Since it is a deep bay (>100 m), when imposing a maximum water depth of 30 m, the resource is highly constrained to the coast and reduced to 145.1 TWh, with an average of 71.5 kW/m^2 (with the 50 kWh/m^2 threshold also applied).

The southern section of the Patagonian shelf contains the major portion of the theoretical resource. In this region, extending from the north of Bahía Grande to Río Grande, where the largest M2 amplitudes occur, the average energy density is 73.1 kWh/m^2, reaching a maximum of 133.5 kWh/m^2 and contributing 4843.7 TWh (39%) of the total unconstrained theoretical resource. Given the bathymetry of the bay, we find that the resource is not reduced to a small section along the coast as in GSM, but it extends further into the bay when the bathymetric constraint is applied. The total resource in this area (<30 m depth and >50 kWh/m^2) is finally calculated at 764.9 TWh, 84% of the total. The southern section can be further subdivided into the areas at either side of the Strait of Magellan: Bahía Grande (BG) and Tierra del Fuego (TdF). The resource maps alone do not provide any information about the timing of the tides; however, referring back to the co-tidal chart for the M2 tide (Fig. 3a), we observe a phase difference between BG and TdF of up to 3 h.

It should be noted there is an area within the Strait of Magellan that experiences a large tidal range (3 m amplitude for M2) which leads to a high energy density area (ca. 95 kWh/m^2 on average). However, despite meeting the bathymetric and annual yield constraints and being on the Patagonian shelf, it has been excluded because it is in the Chile EEZ and it is one of the principal shipping routes between the Atlantic and the Pacific, and therefore it is extremely unlikely that this area would be exploited for renewable energy.

Table 4
The three sites considered for tidal power plant operation models in the Argentinian Patagonia. Other international options from the UK, Mexico and Australia are included for comparison. The mean tidal range $\bar{R}$ and available potential energy per area $E_{\max}/A$ are based on the year 2020 at the selected sites.

Site	Latitude	Longitude	$\bar{R}$ (m)	$E_{\max}/A$ (kWh/m²)	C/A (MW/km²)
Argentina, Patagonia (this study)					
Golfo San Matías	41.67°S	65.00°W	5.86	70.25	15.45
Río Gallegos	51.53°S	68.93°W	7.59	119.99	25.93
Bahía de San Sebastián	53.20°S	68.30°W	6.70	93.60	20.17
Mexico [42]					
San Felipe	31.08°N	114.74°W	4.34	43.65	8.49
Gulf of Santa Clara	31.48°N	114.47°W	4.56	48.15	9.36
Australia [10]					
King Sound	16.89°S	123.65°E	6.75	101.30	20.46
Joseph Bonaparte Gulf	14.77°S	128.77°E	5.37	61.64	12.99
United Kingdom [32,37]					
Swansea	51.57°N	3.98°W	6.60	92.56	19.61
Cardiff	51.45°N	3.15°W	8.56	154.14	32.96
Llandudno	53.33°N	3.83°W	5.65	66.44	14.38

Table 5
Summary of energy conversion predicted through 0D modelling for alternative operation strategies that feature an optimised operation per each tidal cycle.

Name	Operation	E/A (kWh/m²)	η (%)	C_F (%)
Golfo San Matías	Two-way	27.98	39.84	20.69
	Two-way & pumping	32.07	44.66	23.71
Río Gallegos	Two-way	51.44	42.87	22.66
	Two-way & pumping	58.71	48.93	25.86
Bahía de San Sebastián	Two-way	38.74	41.38	21.93
	Two-way & pumping	43.66	46.65	24.72

4.1.2. Technically extractable resource

In delivering a perspective for the extractable resource at potential sites in Fig. 7, we shortlisted three potential locations; (a) Golfo San Matías in the northern part of Patagonia (Fig. 7b), (b) Río Gallegos and (c) Bahía de San Sebastián, with both of the latter in southern Patagonia (Fig. 7c). For the reconstructed signal of an arbitrary year (2020), Table 4 summarises the mean range $\bar{R}$, the available potential energy density $PE = E_{\max}/A$ (Eq. (2)) and normalised capacity factor C/A, based on Eq. (3). In providing a comparative basis on a global scale, the table includes results from other sites in the UK [32], Mexico [42], and Australia [10]. In all cases, we optimised tidal power plant operation and design across all sites based on the same criteria and assumptions.

An overview of the performance of tidal power schemes is summarised in Fig. 8, which highlights the prominence of Patagonia's sites relative to alternative locations. In general, plant operation simulation results indicate that considering optimised scheduling harnessed between $40 - 50\%$ of the available resource. This is consistent with sites in the Severn Estuary and Bristol Channel, which has been regarded as a prime candidate site with multiple studies exploring the feasibility of schemes such as the Severn Barrage [38] and the Swansea Bay tidal lagoon [2]. In addition, the consideration of two-way operation, pumping and a degree of optimisation pushes the capacity factor $C_F > 20\%$, as in Table 5, while still preserving a high degree of efficiency.

Of particular interest is how the three sites in Patagonia convert power in a complementary manner. This is illustrated in Fig. 9 between Río Gallegos and Bahía de San Sebastián, which feature a ≈ 2.0 h phase difference. In order to place this into context, histograms of the normalised power (P/C) were produced in Fig. 10, observing the extent of power generation in time. Individually, for two-way generation, $\approx 50\%$ of the time is invested in holding to facilitate head differences. When considering two schemes together, this value drops to $<30\%$. If pumping is included, $\approx 10\%$ of the time is dedicated to this mode. In

the case of complementary schemes, power generation in one power plant appears to offset pumping, which could alleviate supply issues when power is redirected for pumping functions. The complementary nature exhibited in Patagonia is superior to case studies that have been examined in the UK, where the mitigation of no-conversion periods is more modest when looking at a combination of a scheme in the Severn Estuary, UK (i.e. Cardiff) and along the North Wales coast (i.e. Llandudno). In addition, contrary to the UK, the third site in Patagonia (Golfo San Matías) with a ≈ 2.5 h phase difference from Bahía de San Sebastián is further complementary – with sites across all three locations contributing to the reduction of no-generation periods. It is interesting to note how for the case of two-way generation with pumping, only 12% of the time is dedicated to holding across the sites.

5. Discussion

Tidal power plant operation modelling aspects

In our 0D modelling of tidal power plants in Patagonia, some broad assumptions are included to establish comparative hypothetical scenarios. Some of these assumptions would have conflicting impact for energy conversion predictions. As an example, we assumed that intertidal areas are negligible and the surface area within the impoundment remains constant. This assumption can be questionable in tidally-resonant estuarine regions that feature large expanses of intertidal zones of ecological interest. These areas would require additional construction costs to ensure the expected water volume is impounded, whilst impacting the ratio of energy conversion during ebb/flood regimes. Considering the physics of tidal waves, shallow water regions add substantial resistance to wave and flow propagation, compromising the constant water elevation surface assumption in 0D, requiring hydrodynamically-constrained optimisation to predict robust
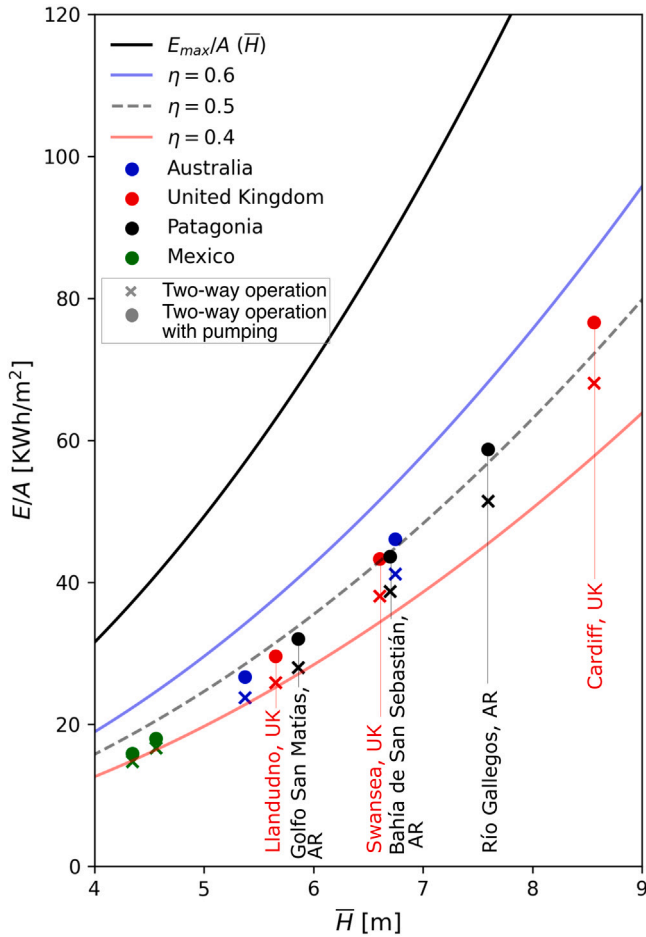
Fig. 8. Comparative performance of sites in Patagonia, relative to international case studies (at UK, AU, MX), in terms of annual available E_{max}/A, and technically extractable energy E/A assuming that schemes are designed and operated based on the same parameters.

scheduling parameters. This assumption would lead to an overestimation of the energy conversion. On the other hand, the conservative turbine design by Aggidis and Feather [34] used for the Hill charts of our analysis, omits advances over a couple of decades that would lead to more efficient energy extraction that could likely exceed 60% of the available energy (see Fig. 8), if the turbine and caisson geometry are optimised. The same applies with the simplified parameterisation of pumping that followed Yates et al. [45] in the absence of state-of-the-art information.

A key opportunity associated with the tides of Patagonia is the benefit of phasing differences (Fig. 10e,f). Individual schemes may have no-generation periods that exceed 50%, but the complementary operation of hypothetical schemes in Patagonia could bring this ratio to 20% without any necessary optimisation (for the case of two-way generation without pumping). This percentage could be minimised further following the example of Mackie et al. [7] who investigated the benefit of phasing differences between the Severn Estuary and the North Wales coast in the UK, and incentivised the operation towards some baseline supply. Whilst this complementarity is often raised as an advantage of tidal energy over intermittent and non-predictable technologies, it is rarely factored into subsidy competition calculations for renewables. Arguably, this is because providing a baseline supply compromises the overall energy output of a scheme, notably impacting metrics such as the Levelised Cost of Energy. Therefore, optimising

further based on this incentive was not considered, beyond mentioning the innate advantage that sites in Patagonia possess.

Financial feasibility

We demonstrate that the metrics for Patagonia are competitive with prime hot spots, with Río Gallegos and San Sebastián exceeding the resource of the most recent Swansea Bay tidal lagoon scheme that was successful in gaining the initial UK Government support to proceed to the formal planning stages. A useful indicator of the technical feasibility of a tidal range scheme is the capacity over impoundment area C/A (Table 4). The impoundment length itself is one of the driving capital cost components that hinders such components. Assuming an ideal scenario of circular offshore (i.e. the entire perimeter is artificial) lagoons of radius r and a constant depth, we can observe the cost associated with the impoundment length. Relative to the resource in Swansea Bay, the impoundment cost of an equivalent capacity at Río Gallegos and San Sebastián would be 15% and 2% cheaper, respectively, while a scheme in Golfo San Matías would be ≈9% more expensive. However, exploiting the bathymetry and coastline through spatial optimisation of the impoundment would effectively define the construction feasibility at these sites.

Practical resource

Patagonia is an extremely biodiverse region and, as such, has many protected areas (Fig. 2b) [46]. These range from UNESCO biosphere reserves and RAMSAR sites to regionally and locally protected areas. As an example, the Patagonia Azul biosphere reserve (north of Golfo San Jorge) is a breeding sanctuary for many birds and mammals, and hosts the largest colony of Magellanic penguins in the world. These protected areas, together with the electricity grid and population areas, have been the main practical limitations taken into account for this study. With this in mind, three sites were chosen to further explore and optimise using different power plant configurations. In GSM, although the resource is higher in the northwestern corner of the bay, it has been disregarded as it overlaps with several protected areas. Additionally, there is a connection to the SADI (132 kV) at Punta Colorada, an old uninhabited iron ore loading port. This existing infrastructure and port could be useful for minimising both the footprint and the cost of any potential projects. The BG area only presents conflicts with protected areas in the northern part. Additionally, in the northern section there are no large, urbanised areas and no connection to the electricity transmission network. On the other hand, in the southern part we find one of the biggest cities in the Patagonian region, Río Gallegos (96,000), which is connected to the SADI through a 220 kV cable. As mentioned earlier, the archipelago of Tierra del Fuego is not connected to the grid. There are two small independent distribution grids around the two main cities: Río Grande (70,000) and Ushuaia (57,000). The theoretical resource is slightly higher towards the north of this section, hence the chosen area is the Bahía de San Sebastián. Regarding protected areas, there is an onshore coastal strip from San Sebastián to Río Grande that is classed as a RAMSAR site, which could pose difficulties in the construction of the onshore parts of a tidal lagoon.

It is likely that a subsea cable will be installed in the future in the Strait of Magellan to connect Tierra del Fuego to the mainland. One of the motivations for this is being able to industrialise hydrocarbons, i.e. electrify the natural gas sourced locally and transport it to the rest of the country. A great part of Tierra del Fuego is in the Austral basin, one of the five active production basins in the country. This also means there will be some competition between tidal renewable energy and oil and gas production, but also some existing infrastructure in the area that could be shared or reused. Additionally, the southern sites in particular, also present an opportunity for offshore consumption, for example, a charging point for hybrid and electric vessels sailing through the Strait.
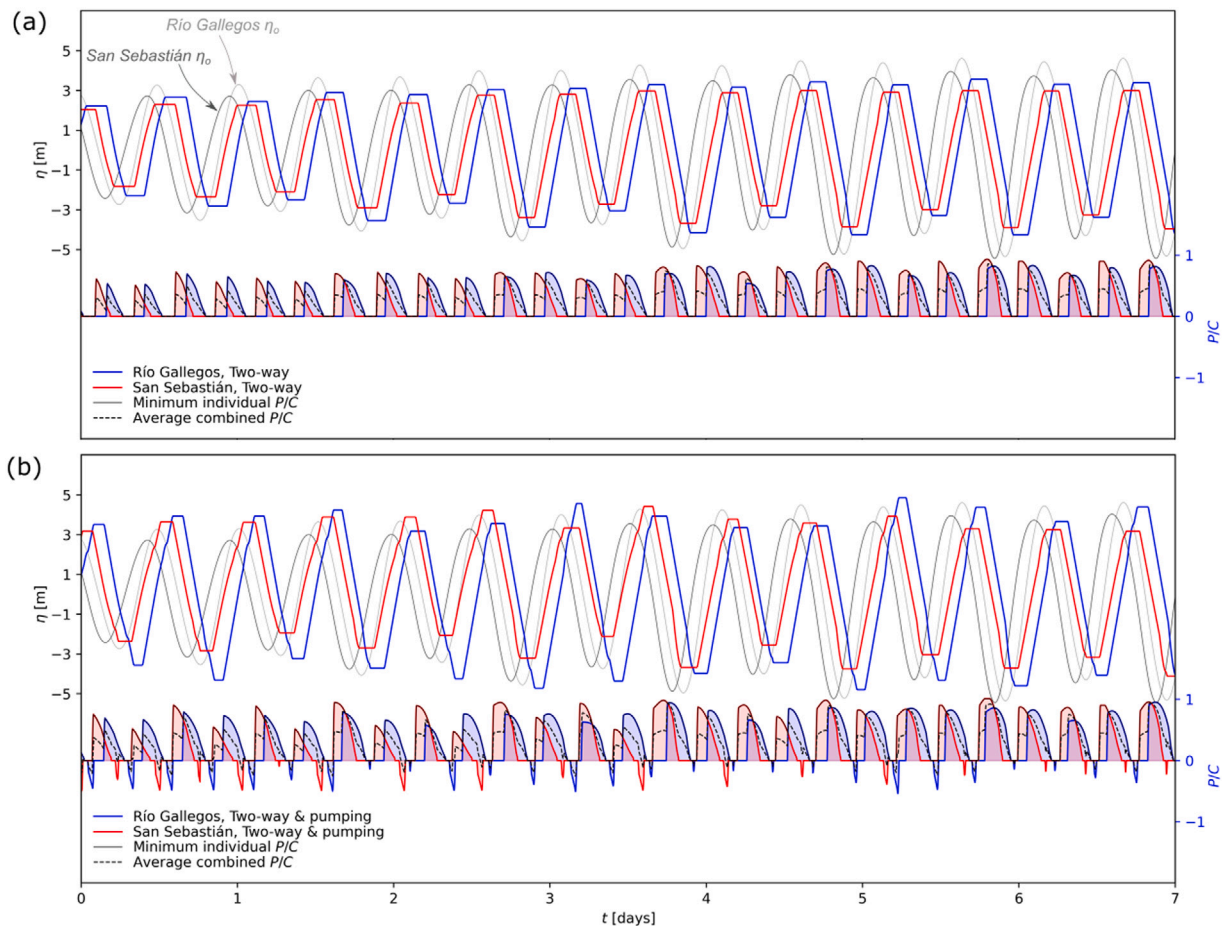
Fig. 9. Tidal power plant operation over a transition from neap to spring tide for sites of complementary phase (Río Gallegos and San Sebastían).

Sea-level rise

Global model simulations that include sea-level rise have demonstrated that a 2 m uniform increase in global mean sea level would lead to modest reduction (around 2 cm) in S2 tidal amplitudes in the Golfo San Matías, with almost no change in amplitudes of the M2, K1 and O1 constituents [47]. Research focused on the Patagonian shelf for a larger change in sea level (3 m) shows that the effect on tidal amplitudes in the region is patchy, but could be in the range ±20 cm, especially in the Golfo San Matías and Bahía Blanca [48]. To investigate this further, we extracted a bathymetry profile extending out from the Golfo San Jorge to the location of the local M2 amphidromic point (a distance of 370 km). With present day water depths along the profile (mean 68 m), the mean phase speed c is 25 m/s, and so for (M2) quarter wave length resonance [2], $L/4 = 280.1$ km. With a sea-level rise (SLR) scenario of either 1 m or 2 m, the corresponding $L/4$ would increase to 282.4 m or 284.8 m, respectively, bringing the system closer to resonance and so theoretically increasing the M2 amplitude in the Golfo San Matías. Since the S2 amphidromic point is closer to the Golfo San Matías (Fig. 3), this could explain why Pickering et al. [47] found the S2 constituent to be more responsive to SLR in this region. Repeating the calculation for S2, $L/4$ for the S2 constituent is currently 270.3 km – very close to the actual distance, 278 km of the amphidromic point from the Golfo San Matías. With a SLR of 1 m (2 m), $L/4$ increases to 272.7 km (275.0 km), bringing the system even closer to resonance. Of course the actual system is more complex than this, as the global tides (and hence the location of the amphidromic points) would change due to sea-level rise [47]; however these calculations demonstrate that the tidal range resource would likely increase in this region in the future.

6. Conclusion

Tidal resonance along the Patagonian coast leads to very high tidal ranges (up to 8 m), which could further increase with sea-level rise. This means the Patagonian shelf is a hot spot for tidal range energy. The theoretical resource (constrained by water depths less than 30 m) is 913 TWh, and concentrated in two main areas. When considering the practical limitations, three sites stand out as feasible for development, with grid connection and protected sites being the biggest constraints. As for the technical resource, Río Gallegos is found to perform extremely well compared to other international case studies. Additionally, the performance can be enhanced by optimising sites that are complementary in phase, presenting opportunities for a more uniform generation profile and minimising periods of no-generation. The analysis comparing with international case studies with equivalent operation suggests this complementarity is a distinctively greater opportunity due to the phasing of tides in Patagonia. This is based on an assumption of a relatively close proximity of the sites in question to a centralised electrical grid across Argentina. Considering the increasing interest in the concept of a tidal lagoon (smaller scale), the technological advances in turbine regulation and pumping, and the prospect of a strategically developed electrical grid, these conditions could mean that tidal range power plants could again be on the table for Argentina. Further work could involve the development of regional models for better understanding feedbacks (e.g. including wind and waves, as well as interactions with marine habitats) and reducing uncertainties and assumptions regarding the tidal dynamics in shallow water. In particular, regional models can be used to optimise the sites from a
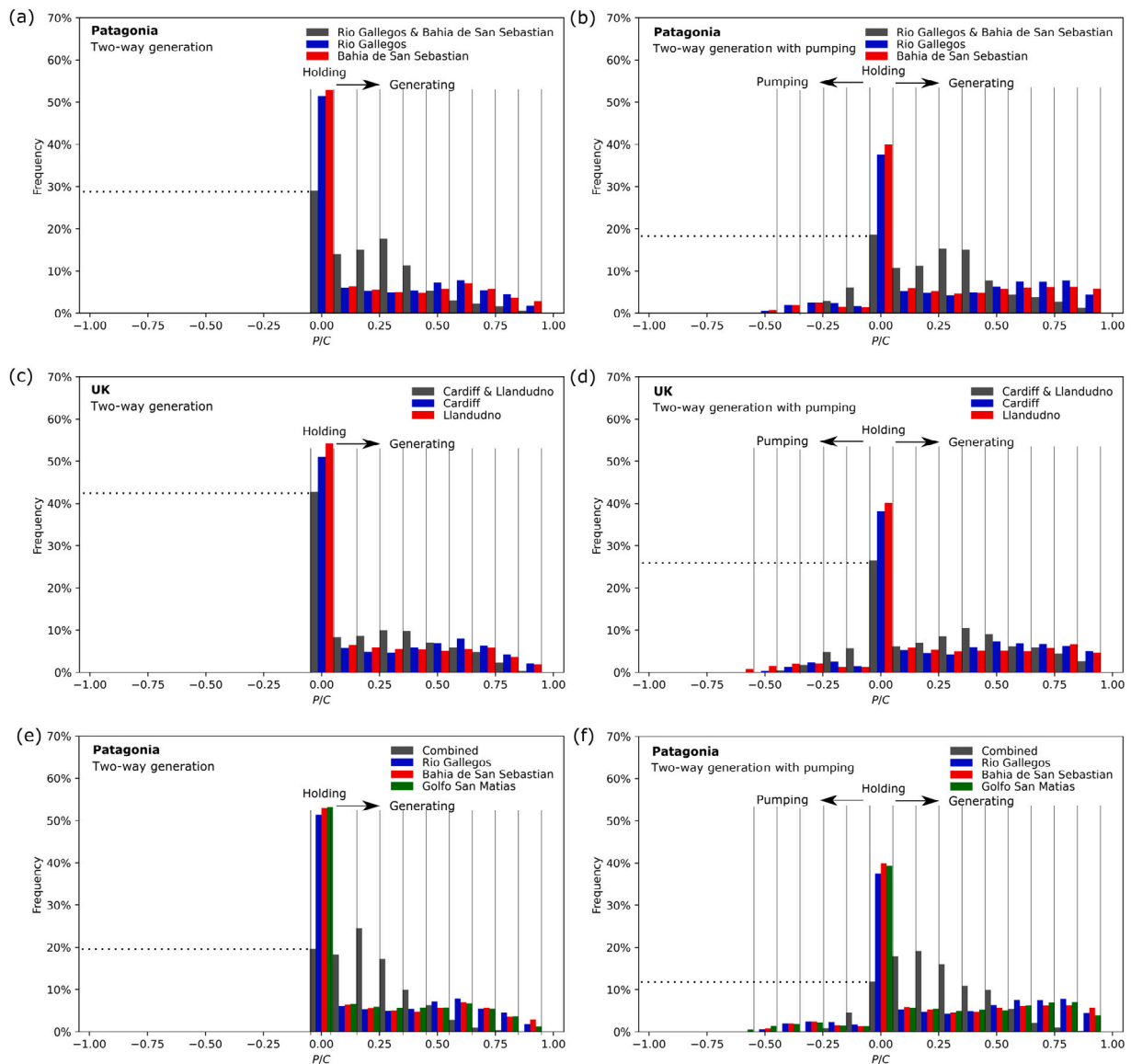
Fig. 10. Histogram of normalised power output from operation of tidal power plants at complementary sites for two optimised operation strategies. (a) Two-way generation and (b) Two-way generation with pumping at two sites at Patagonia. (c) Two-way generation and (d) Two-way generation with pumping based on UK sites. (a) Two-way generation and (b) Two-way generation with pumping at three sites at Patagonia. Power generation profiles are considered for each site separately (blue/red/green), and in combination (grey).

spatial perspective which would inform on the potential capital costs of the lagoons.

CRediT authorship contribution statement

Vicky Martí Barclay: Conceptualization, Methodology, Formal analysis, Writing – original draft, Visualization. **Simon P. Neill:** Conceptualization, Methodology, Formal analysis, Writing – original draft, Funding acquisition. **Athanasios Angeloudis:** Methodology, Formal analysis, Writing – original draft, Funding acquisition.

Declaration of competing interest

The authors declare that they have no known competing financial interests or personal relationships that could have appeared to influence the work reported in this paper.

Acknowledgements

References

[1] IEA electricity, 2022, https://www.iea.org/fuels-and-technologies/electricity, Accessed: 2022-12-01.

[2] S. Neill, K. Haas, J. Thiebot, Z. Yang, A review of tidal energy-resource, feedbacks, and environmental interactions, J. Renew. Sustain. Energy (2021) http://dx.doi.org/10.1063/5.0069452.

[3] S.P. Neill, A. Angeloudis, P.E. Robins, I. Walkington, S.L. Ward, I. Masters, M.J. Lewis, M. Piano, A. Avdis, M.D. Piggott, et al., Tidal range energy resource and optimization–past perspectives and future challenges, Renew. Energy 127 (2018) 763–778, http://dx.doi.org/10.1016/j.renene.2018.05.007.

[4] T. McErlean, Harnessing the Tides, the Early Medieval Tide Mills at Nendrum Monastery, Strangford Lough, in: Northern Ireland Archaeological Monographs, No 7, The Stationery Office, 2007.

[5] R.H. Charlier, Forty candles for the Rance river TPP tides provide renewable and sustainable power generation, Renew. Sustain. Energy Rev. 11 (9) (2007) 2032–2057, http://dx.doi.org/10.1016/j.rser.2006.03.015.

[6] J. Wolf, I.A. Walkington, J. Holt, R. Burrows, Environmental impacts of tidal power schemes, in: Proc. Inst. Civ. Eng. Maritime Eng., 162, (4) Thomas Telford Ltd, 2009, pp. 165–177.

[7] L. Mackie, D. Coles, M. Piggott, A. Angeloudis, The potential for tidal range energy systems to provide continuous power: A UK case study, J. Mar. Sci. Eng. 8 (10) (2020) http://dx.doi.org/10.3390/jmse8100780.

[8] G. Egbert, R. Ray, Significant dissipation of tidal energy in the deep ocean inferred from satellite altimeter data, Nature 405 (6788) (2000) 775–778, http://dx.doi.org/10.1038/35015531.

[9] D. Hasegawa, J. Sheng, D.A. Greenberg, K.R. Thompson, Far-field effects of tidal energy extraction in the Minas passage on tidal circulation in the Bay of Fundy and Gulf of Maine using a nested-grid coastal circulation model, Ocean Dyn. 61 (11) (2011) 1845–1868, http://dx.doi.org/10.1007/s10236-011-0481-9.

[10] S.P. Neill, M. Hemer, P.E. Robins, A. Griffiths, A. Furnish, A. Angeloudis, Tidal range resource of Australia, Renew. Energy 170 (2021) 683–692, http://dx.doi.org/10.1016/j.renene.2021.02.035.

[11] M.R. Chingotto, Energía mareomotriz. ¿Sí? ¿Dónde? ¿No? ¿Por qué? Conclusiones, Boletín Centro Naval (2006).

[12] A.P. Federico, Las posibilidades de aprovechamientos mareomotrices en la República Argentina, Rev. 89 Univ. Nac. Lit. (89) (1978) 84–101.

[13] Informe anual, 2021, https://cammesaweb.cammesa.com/informe-anual/. Accessed: 2021-10-05.

[14] P. Glorioso, J. Simpson, Numerical modelling of the M2 tide on the northern Patagonian shelf, Cont. Shelf Res. 14 (2) (1994) 267–278, http://dx.doi.org/10.1016/0278-4343(94)90016-7.

[15] P.D. Glorioso, R.A. Flather, A barotropic model of the currents off SE south America, J. Geophys. Res.: Oceans 100 (C7) (1995) 13427–13440, http://dx.doi.org/10.1029/95JC00942.

[16] P.D. Glorioso, R.A. Flather, The Patagonian shelf tides, Prog. Oceanogr. 40 (1–4) (1997) 263–283, http://dx.doi.org/10.1016/S0079-6611(98)00004-4.

[17] P.D. Glorioso, Patagonian shelf 3D tide and surge model, J. Mar. Syst. 24 (1) (2000) 141–151, http://dx.doi.org/10.1016/S0924-7963(99)00084-6.

[18] C. Simionato, W. Dragani, M. Nuñez, M. Engel, A set of 3-D nested models for tidal propagation from the Argentinean continental shelf to the Rio de La Plata Estuary—Part I. M2, J. Coast. Res. 20 (3) (2004) 893–912.

[19] D. Moreira, C. Simionato, W. Dragani, Modeling ocean tides and their energetics in the north Patagonia gulfs of Argentina, J. Coast. Res. 27 (1) (2011) 87–102.

[20] Instituto Geográfico Nacional, 2022, https://www.ign.gob.ar/. Accessed: 2022-10-12.

[21] D.J. Webb, A model of continental-shelf resonances, Deep Sea Res. Oceanogr. Abstr. 23 (1976) 1–15, http://dx.doi.org/10.1016/0011-7471(76)90804-4.

[22] J.H. Middleton, L. Bode, Poincaré waves obliquely incident to a continental shelf, Cont. Shelf Res. 7 (2) (1987) 177–190, http://dx.doi.org/10.1016/0278-4343(87)90078-1.

[23] V. Buchwald, Resonance of poincaré waves on a continental shelf, Mar. Freshw. Res. 31 (4) (1980) 451–457, http://dx.doi.org/10.1071/MF9800451.

[24] B.K. Arbic, R.H. Karsten, C. Garrett, On tidal resonance in the global ocean and the back-effect of coastal tides upon open-ocean tides, Atmos.-Ocean 47 (4) (2009) 239–266, http://dx.doi.org/10.3137/OC311.2009.

[25] S.L. Ward, P.E. Robins, M.J. Lewis, G. Iglesias, M.R. Hashemi, S.P. Neill, Tidal stream resource characterisation in progressive versus standing wave systems, Appl. Energy 220 (2018) 274–285, http://dx.doi.org/10.1016/j.apenergy.2018.03.059.

[26] P.E. Robins, S.P. Neill, M.J. Lewis, S.L. Ward, Characterising the spatial and temporal variability of the tidal-stream energy resource over the northwest European shelf seas, Appl. Energy 147 (2015) 510–522, http://dx.doi.org/10.1016/j.apenergy.2015.03.045.

[27] G.D. Egbert, S.Y. Erofeeva, Efficient inverse modeling of barotropic ocean tides, J. Atmos. Ocean. Technol. 19 (2) (2002) 183–204, http://dx.doi.org/10.1175/1520-0426(2002)019<0183:EIMOBO>2.0.CO;2.

[28] I.D. Haigh, M. Marcos, S.A. Talke, P.L. Woodworth, J.R. Hunter, B.S. Hague, A. Arns, E. Bradshaw, P. Thompson, GESLA version 3: A major update to the global higher-frequency sea-level dataset, Geosci. Data J. (2022) http://dx.doi.org/10.1002/gdj3.174.

[29] P.L. Woodworth, J.R. Hunter, M. Marcos, P. Caldwell, M. Menéndez, I. Haigh, Towards a global higher-frequency sea level dataset, Geosci. Data J. 3 (2) (2016) 50–59, http://dx.doi.org/10.1002/gdj3.42.

[30] R. Pawlowicz, B. Beardsley, S. Lentz, Classical tidal harmonic analysis including error estimates in MATLAB using T_TIDE, Comput. Geosci. 28 (8) (2002) 929–937, http://dx.doi.org/10.1016/S0098-3004(02)00013-4.

[31] K. Pappas, L. Mackie, I. Zilakos, A.H. van der Weijde, A. Angeloudis, Sensitivity of tidal range assessments to harmonic constituents and analysis timeframe, Renew. Energy 205 (2023) 125–141, http://dx.doi.org/10.1016/j.renene.2023.01.062.

[32] A. Angeloudis, S.C. Kramer, A. Avdis, M.D. Piggott, Optimising tidal range power plant operation, Appl. Energy 212 (2018) 680–690, http://dx.doi.org/10.1016/j.apenergy.2017.12.052.

[33] A. Angeloudis, L. Mackie, M.D. Piggott, Tidal range energy, in: T.M. Letcher (Ed.), Comprehensive Renewable Energy (Second Edition), second ed., Elsevier, Oxford, 2022, pp. 80–103.

[34] G. Aggidis, O. Feather, Tidal range turbines and generation on the solway firth, Renew. Energy 43 (2012) 9–17, http://dx.doi.org/10.1016/j.renene.2011.11.045.

[35] A. Angeloudis, S.C. Kramer, N. Hawkins, M.D. Piggott, On the potential of linked-basin tidal power plants: An operational and coastal modelling assessment, Renew. Energy 155 (2020) 876–888, http://dx.doi.org/10.1016/j.renene.2020.03.167.

[36] R. Burrows, I. Walkington, N. Yates, T. Hedges, J. Wolf, J. Holt, The tidal range energy potential of the West Coast of the United Kingdom, Appl. Ocean Res. 31 (4) (2009) 229–238, http://dx.doi.org/10.1016/j.apor.2009.10.002.

[37] A. Angeloudis, R. Falconer, S. Bray, R. Ahmadian, Representation and operation of tidal energy impoundments in a coastal hydrodynamic model, Renew. Energy 99 (2016) 1103–1115, http://dx.doi.org/10.1016/j.renene.2016.08.004.

[38] J. Xia, R.A. Falconer, B. Lin, G. Tan, Estimation of annual energy output from a tidal barrage using two different methods, Appl. Energy 93 (2012) 327–336, http://dx.doi.org/10.1016/j.apenergy.2011.12.049.

[39] A. Angeloudis, R.A. Falconer, Sensitivity of tidal lagoon and barrage hydrodynamic impacts and energy outputs to operational characteristics, Renew. Energy 114(A) (2017) 337–351, http://dx.doi.org/10.1016/j.renene.2016.08.033.

[40] L. Mackie, S.C. Kramer, M.D. Piggott, A. Angeloudis, Assessing impacts of tidal power lagoons of a consistent design, Ocean Eng. 240 (2021) 109879, http://dx.doi.org/10.1016/j.oceaneng.2021.109879.

[41] A.L. Baker, R.M. Craighead, E.J. Jarvis, H.C. Stenton, A. Angeloudis, L. Mackie, A. Avdis, M.D. Piggott, J. Hill, Modelling the impact of tidal range energy on species communities, Ocean Coast. Manage. 193 (2020) 105221, http://dx.doi.org/10.1016/j.ocecoaman.2020.105221.

[42] C.J. Mejia-Olivares, I.D. Haigh, A. Angeloudis, M.J. Lewis, S.P. Neill, Tidal range energy resource assessment of the Gulf of California, Mexico, Renew. Energy 155 (2020) 469–483, http://dx.doi.org/10.1016/j.renene.2020.03.086.

[43] F. Harcourt, A. Angeloudis, M.D. Piggott, Utilising the flexible generation potential of tidal range power plants to optimise economic value, Appl. Energy 237 (2019) 873–884, http://dx.doi.org/10.1016/j.apenergy.2018.12.091.

[44] S.P. Neill, M.R. Hashemi, Chapter 5 - wave energy, in: S.P. Neill, M.R. Hashemi (Eds.), Fundamentals of Ocean Renewable Energy, in: E-Business Solutions, Academic Press, 2018, pp. 107–140, http://dx.doi.org/10.1016/B978-0-12-810448-4.00005-7.

[45] N. Yates, I. Walkington, R. Burrows, J. Wolf, The energy gains realisable through pumping for tidal range energy schemes, Renew. Energy 58 (2013) 79–84, http://dx.doi.org/10.1016/j.renene.2013.01.039.

[46] M. Shadman, M. Roldan-Carvajal, F.G. Pierart, P.A. Haim, R. Alonso, C. Silva, A.F. Osorio, N. Almonacid, G. Carreras, M. Maali Amiri, S. Arango-Aramburo, M.A. Rosas, R. Pelissero, R. Tula, S.F. Estefen, M.L. Pastor, O.R. Saavedra, A review of offshore renewable energy in South America: Current status and future perspectives, Sustainability 15 (2) (2023) http://dx.doi.org/10.3390/su15021740.

[47] M. Pickering, K. Horsburgh, J. Blundell, J.-M. Hirschi, R.J. Nicholls, M. Verlaan, N. Wells, The impact of future sea-level rise on the global tides, Cont. Shelf Res. 142 (2017) 50–68, http://dx.doi.org/10.1016/j.csr.2017.02.004.

[48] S.J. Carless, J.M. Green, H.E. Pelling, S.-B. Wilmes, Effects of future sea-level rise on tidal processes on the Patagonian shelf, J. Mar. Syst. 163 (2016) 113–124, http://dx.doi.org/10.1016/j.jmarsys.2016.07.007.